Geoscience Frontiers 12 (2021) 101113

HOSTED BY

Contents lists available at ScienceDirect

Geoscience Frontiers

journal homepage: www.elsevier.com/locate/gsf

Research Paper

Tectonic evolution of the Karakoram metamorphic complex (NW Himalayas) reflected in the 3D structures of spiral garnets: Insights from X-ray computed micro-tomography

M. Sayab [a,*], D. Aerden [b], J. Kuva [a], W.U. Hassan [c]

[a] Geological Survey of Finland, P.O. Box 96, FI-02151 Espoo, Finland
[b] Departamento de Geodinámica and IACT-CSIC, Universidad de Granada, Granada 18002, Spain
[c] National Centre of Excellence in Geology, University of Peshawar, Peshawar 25130, Pakistan

ARTICLE INFO

Article history:
Received 2 July 2020
Received in revised form 10 September 2020
Accepted 12 November 2020
Available online 15 December 2020

Handling Editor: Richard M. Palin

Keywords:
Porphyroblast
Garnet
FIA
X-ray tomography
Karakoram
Himalayas

ABSTRACT

Spiral garnet porphyroblasts are known to record lengthy periods of deformation and metamorphism by preserving single or multiple FIAs (Foliation Intersection Axis) formed normal to tectonic shortening directions. Thanks to technological advances in X-ray computed micro-tomography (XCMT), FIAs can now be readily determined in relatively large samples in contrast to previous methods that require the preparation of a set of radial vertical and horizontal thin sections of samples. XCMT scanning not only alleviates tedious thin section based procedures but also illuminates the complete internal architecture of a rock sample allowing three-dimensional (3D) quantitative shape analysis of an individual porphyroblast as well as precise measurement of FIAs. We applied the technique to a sample from the Hunza Valley in the Karakoram metamorphic complex (KMC), NW Himalayas, containing numerous garnet porphyroblasts with spiral-shaped inclusion trails. The XCMT imaging reveals an E–W trending FIA within the sample, which is consistent with orthogonal N–S collision of the India-Kohistan Island Arc with Asia. Garnet long axes (X_{GT}) have variable plunges that define a broad sub-vertical maximum and a small sub-horizontal maximum. The X_{GT} principle maxima lie at N-090 and N-120. Smaller maxima lie at N-020 and N-340. Geometric relationships between X_{GT} axes and FIA orientation in the sample suggest that porphyroblast shapes are controlled by the geometry of the lens-shaped microlithons in which they tend to nucleate and grow. The orientation of inclusion trails and matrix foliations in the sample are correlated with three discrete tectono-metamorphic events that respectively produced andalusite, sillimanite and kyanite in the KMC. Late staurolite growth in the sample reveals how the rocks extruded to the surface via a significant role of roll-on tectonics, which can be correlated with the Central Himalayas.

1. Introduction

A Foliation Intersection/Inflection Axis (FIA) is the curvature axis or symmetry axis of inclusion trails with sigmoidal or spiral shape preserved within porphyroblasts. Hayward (1990) and Bell et al. (1995) devised a method to measure the average orientation of FIAs in a sample by recording the asymmetry (i.e. curvature sense) of inclusion trails in radial sets of thin sections. Two contrasting genetic models have been proposed for such inclusion trails and attribute a different tectonic significance to FIAs. The earlier of these models (e.g. Rosenfeld, 1970; Dixon, 1976; Schoneveld, 1977; Powell and Vernon, 1979; Passchier et al., 1992; Williams and Jiang, 1999; Jiang and Williams, 2004) explain them by shearing-induced rotation of growing porphyroblasts, whereas the more recent model (e.g. Bell et al., 1986, 1992; Bell and Johnson, 1989; Aerden, 1995; Sayab, 2005; Aerden and Ruiz-Fuentes, 2020) envisages a formation by overgrowth of actively developing crenulation hinges that become fixed in non-rotating porphyroblasts. In the first model, the amount of inclusion-trail curvature depends on the shear strain and flow vorticity. In the second model, it is a function of the number of deformation phases and accompanying porphyroblast growth stages.

FIAs have been shown to have regionally consistent orientations in orogenic belts and to represent early fold trends that can generally not be deduced from the matrix foliation (e.g. Timms, 2003; Bell and Sanislav, 2011). Therefore, FIA provide valuable constraints on regional-scale kinematic reconstructions (e.g. Aerden, 2004; Sayab, 2008; Shah et al., 2011). This paper focuses on the relationships between FIA and the 3D shape of garnet porphyroblasts in a relatively large (ca. 114 cm^3) sample from the Hunza Valley of the Karakoram metamorphic complex (KMC), NW Himalayas, Pakistan. Detailed petrographic examination of the sample combined with X-ray computed

* Corresponding author.
E-mail address: sayab.muhammad@gtk.fi (M. Sayab).

https://doi.org/10.1016/j.gsf.2020.11.010

micro-tomography (XCMT) analysis of garnet shapes and orientations allow us to evaluate whether the inclusion trails formed by a single phase of shearing-induced porphyroblast rotation or alternatively by successive folding events that re-oriented the matrix foliation relative to stable porphyroblasts. It will be shown that the non-rotation model predicts the sub-vertical preferred orientation of garnet long axes demonstrated in the sample perpendicular to sub-horizontal FIAs, plus orthogonal truncation surfaces associated with the inclusion trails when viewed in FIA-perpendicular sections. The succession of near-orthogonal geometry of foliations preserved within the spiral garnet porphyroblasts not only reflects the folding history in response to multiple stages of compression and decompression of the orogen, but also highlights the previously established metamorphic sequence of andalusite, followed by sillimanite and its replacement by kyanite that accompanied the amalgamation of India, the Kohistan Island Arc, and Asia (Fraser et al., 2001; Palin et al., 2012). Younger staurolite porphyroblasts in the sample preserve inclusion trails with an opposite sense of shear as compared to the garnet porphyroblasts, which can be explained via the key role of roll-on tectonics (Bell and Newman, 2006) that extruded the rocks to the surface by gravity-induced thrusting.

1.1. FIA background

FIA represents the axis of curvature and/or of internal truncation of sigmoidal to complex spiral-shaped inclusion trails preserved within porphyroblasts (Fig. 1; Hayward, 1990). FIA orientations have been found to be regionally consistent in numerous orogens and are interpreted to record directions of bulk crustal shortening perpendicular to the FIAs (e.g. Bell et al., 1998; Bell and Welch, 2002; Yeh, 2007; Aerden and Sayab, 2008; Sayab, 2008; Shah et al., 2011; Skrzypek et al., 2011; Aerden et al., 2013; Kim and Sanislav, 2017). Multiple sets of distinctly oriented FIA thus record a succession of different tectonic events that are very difficult, if not impossible, to unravel by only studying fabrics in the matrix (e.g. Aerden, 2004; Ham and Bell, 2004; Sayab, 2005) due to repeated reactivation, reorientation and metamorphic re-equilibration of phyllosilicates in metapelites in response to subsequent deformations (e.g. Kim and Bell, 2005; Sayab, 2006). Nevertheless, careful sample-to-sample microstructural analysis of low-strain zones in the matrix in some cases allowed the reconstruction of the original orientation of strongly overprinted foliations (e.g. Timms, 2003; Aerden and Sayab, 2017). In the Himalayan belts an intriguing temporal and spatial correlation has been found between the trends of successive FIA sets and successive vectors of relative India-Asia plate motions (Shah et al., 2011; Bell and Sapkota, 2012; Sayab et al., 2016) reconstructed from onland and ocean-floor magnetic anomalies (e.g. Patriat and Achache, 1984).

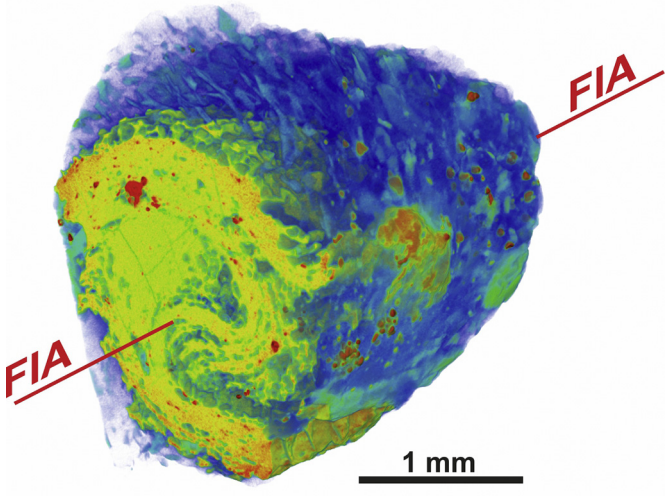

Fig. 1. Three-dimensional (3D) image of a single garnet porphyroblast from the sample W-11 showing spiral inclusion trails. The red line is characterized by the curvature axis or FIA. The garnet was extracted from the sample using SelFrag. The garnet was scanned using an X-ray computed micro-tomography (XCMT) at 80 kV and 63 μA in 2-h yielding a resolution of 5 μm.

Irrespective of whether spiral inclusion trails develop by shearing induced porphyroblast rotation or by stationary porphyroblast episodically overgrowing multiple crenulation cleavages, the FIA that develops is an important kinematic indicator. In the rotation model, it indicates the sense of progressive simple shear on the dominant matrix foliation (e.g. Rosenfeld, 1970; Schoneveld, 1977), whereas the non-rotation model predicts the shear sense history associated with a sequence of sub-vertical and sub-horizontal foliations with near-orthogonal shortening components (Bell et al., 1998; Bell and Sanislav, 2011). Significantly, the shear sense predicted by both models is opposite for any given foliation (cf. Robyr et al., 2009 versus Bell and Fay, 2016).

1.2. Existing FIA determination methods

So far, FIAs have been measured by recording the switch in asymmetry exhibited by inclusion trails in radial thin section sets (Hayward, 1990). The FIA trend can be determined by cutting vertical sections in a radial pattern with an accuracy that depends on their angular spacing, usually between 30° and 10°. The plunge can then be determined by cutting an additional radial set of thin sections about a horizontal axes oriented perpendicular to the FIA trend (Bell et al., 1995), but this is usually not done for practical reasons. Depending on the quality and complexity of the inclusion trails sometimes two or even three sets of FIA can be distinguished included in core, median, and rim zones of porhyroblasts or different porphyroblast minerals present in a sample (e.g. Sayab, 2005; Cihan et al., 2006; Sanislav, 2011). In practical terms, the technique requires a large sized sample, cutting multiple precisely oriented horizontal slabs, marking up the slabs, cutting vertical blocks and preparing thin sections. The whole procedure is a rather tedious and time consuming process only done by structural and metamorphic geologists who have realized the wealth of data that can be obtained from them. Aerden (2003) wrote a computer program ('FitPitch') that calculates best-fit planes and corresponding FIA (intersections of best-fit planes) for pitch measurements of relatively planar inclusion trails in multiple differently oriented thin sections.

Huddlestone-Holmes and Ketcham (2010) imaged 58 garnet porphyroblasts and measured their FIA trends using XCMT. Due to limited scan size at that time, they extracted four 1.1 cm wide and 3 cm long drill cores from the studied sample. This procedure would not have allowed studying porphyroblasts with diameters greater than 1 cm.

1.3. Refined FIA determination method

With the technological advancements of XCMT in the last decade or so, in terms of X-ray power, size of detectors, acquisition times and resolution, relatively large rock samples can now be scanned at a faster rate. The method has started to be applied for 3D spatial analysis of metamorphic textures (e.g. Whitney et al., 2008; Robyr et al., 2009; Sayab et al., 2015; George and Gaidies, 2017) and we envisage that virtual-reality based micro-structural analysis will soon be routinely used since desktop-based XCMT scanners have become increasingly available and affordable. We present a virtual-reality based petrographic study of a rock slab preserving garnet porphyroblasts. Our virtual 3D petrographic tour inside the rock sample as well as numerous 2D virtual slices allowed determination of the average orientation of FIAs in garnet porphyroblasts in the rock slab. We quantified all the garnet porphyroblasts using advanced recipes of ThermoFisher

PerGeos software: https://www.thermofisher.com/fi/en/home/industrial/electron-microscopy/electron-microscopy-instruments-workflow-solutions/3d-visualization-analysis-software/pergeos-digital-rock-analysis.html. Aerden and Ruiz-Fuentes (2020) recently applied a similar method using the ImageJ software on two samples hosting spiral garnets collected from two regional shear-zones.

2. Sample description

Sample W-11 was collected from the Hunza Valley of KMC of the NW Himalayas, Pakistan (GPS co-ordinates: N36°15.760′ and E74° 34.414′). The KMC is composed of marbles, meta-marls and calc-silicates with subordinate metapelites and orthogneiss units (Searle, 1991; Rolland et al., 2006; Searle and Hacker, 2019). The KMC is bounded by the Karakoram Batholith to the north and Shyok Suture Zone to the south, respectively. The Hunza Valley of the KMC consists of a series of south-vergent thrust faults and folds, which are the product of the Eocene India-Asia collision. Metamorphic grade of the Hunza Valley generally increases from the garnet-chloritoid zone to kyanite and sillimanite zone from south to north, respectively (Fraser et al., 2001; Palin et al., 2012).

Sample W-11 is a metapelitic schist containing garnet, staurolite and kyanite porphyroblasts from the lower sillimanite zone of Palin et al. (2012). The lower sillimanite zone is overprinted by kyanite grade metamorphism. It has been interpreted that the peak sillimanite-grade metamorphism within the lower sillimanite zone occurred at 44 ± 2.0 Ma based on the U–Pb monazite ages (Fraser et al., 2001). However, an earlier andalusite grade contact metamorphism and a later kyanite grade overprint have been dated at 105.5 ± 0.8 Ma and 28.2 ± 0.8 Ma, respectively (Palin et al., 2012). The ages have been obtained from a single sample (20-199 of Fraser et al., 2001; Palin et al., 2012) indicating three separate metamorphic episodes characterized by andalusite, sillimanite and late kyanite. Spiral garnet porphyroblasts have been previously reported from the Hunza Valley (Powell and Vernon, 1979).

The strike of the matrix foliation in W-11 is east-west and steeply (70°) dipping towards the north (Fig. 2). The orientation of foliation within this sample is a manifestation of the large-scale east-west striking structures of the Hunza Valley. Garnet porphyroblasts in this sample do not exceed 5 mm in diameter. For XCMT analysis, a slab of 7 cm × 6.5 cm × 2.5 cm was cut (Fig. 2a).

3. XCMT based virtual petrography

XCMT images rock volumes at the micron to nano scale and provides 3D voxel data that can be used to create virtual cross-sections at any desired angle (e.g. Sayab et al., 2017; Suuronen and Sayab, 2018). It also allows the extraction of size, shape and volume data for different minerals present in a rock based on their density contrasts and X-ray energy and can be segmented and separated from the rest of the rock sample (e.g. Ketcham, 2005; Cnudde and Boone, 2013; Fusseis et al., 2014; Hanna and Ketcham, 2017). Generally, garnet porphyroblasts have enough density (3.5–4.1 g/cm^3) contrast with respect to matrix minerals like quartz (2.6 g/cm^3), feldspar (2.5 g/cm^3), calcite (2.7 g/cm^3) and mica (2.8–3.0 g/cm^3) for automatic and quick segmentation (see below).

Sample W-11 was analysed using the recently installed GE phoenix v|tome|x s micro-tomography scanner of the Geological Survey of Finland at Espoo. One of the main features of this instrument is that it is equipped with a dual tube system, a 240 kV directional microfocus tube and a 180 kV transmission nanofocus tube, with a large high-contrast (2024 × 2024 pixel) flat-panel detector GE DXR250. For data acquisition and reconstruction, the instrument came with a phoenix datos|x module package. After reconstructing the XCMT data, we used the PerGeos software from ThermoFisher Scientific for visualization, segmentation, and quantitative analyses. The sample (W-11) was scanned in two independent steps with the microfocus tube. In the first step, the whole sample was scanned, which took about 6 h. The instrument was operated with an acceleration voltage of 175 kV and a tube current of 158 μA. The X-ray radiation was filtered with 0.5 mm of Cu and 0.5 mm Al to reduce beam hardening and enhance contrast. 2700 projections per 360° (step size of 0.13) were acquired in a single scan with a 2 s exposure time. Based on these configurations, the resulting 3D volume has a voxel size of 27 μm. Part of the sample (2.5 cm × 1.5 cm × 2.5 cm, Fig. 2c) was scanned at a higher resolution of 12 μm in order to study inclusion trails in great detail. The high-resolution scan was acquired through 2700 projections with 2 s exposure time (6 h total), 100 kV accelerating voltage, 120 μA tube current, and using a 0.5 mm Cu filter.

3.1. Digital sectioning and FIA determination

Before observing the switch in the asymmetry of inclusion trails to mark the FIA trend, a virtual tour inside the rock volume was made using a high-resolution virtual reality (VR) headset (https://www.

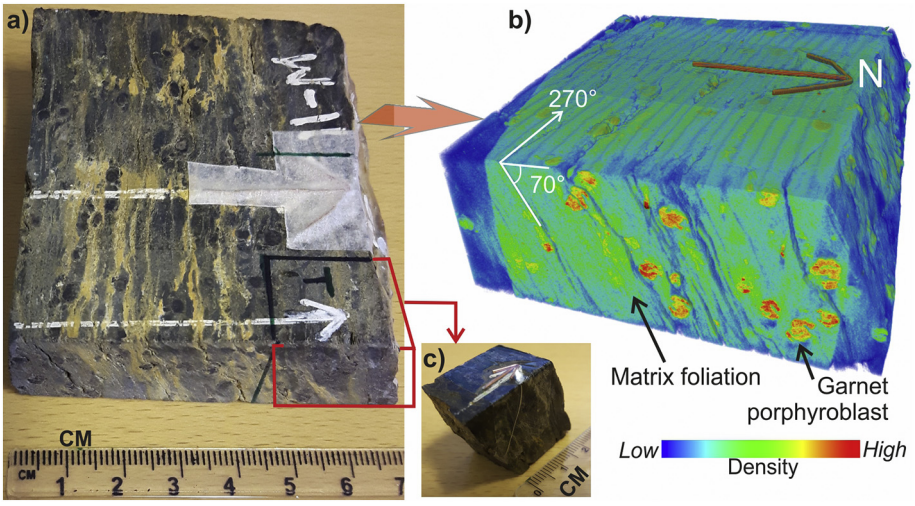

Fig. 2. (a) Oriented slab of sample W-11. North arrow made of brass wire is hidden under the sticky tape. (b) XCMT 3D reconstruction of the sample scanned at 27 μm resolution. Garnet porphyroblasts are rendered in warm colours (red and orange). (c) Small sample piece cut for a higher-resolution scan (cf. Fig. 5a, b). (For interpretation of the references to colour in this figure legend, the reader is referred to the web version of this article).

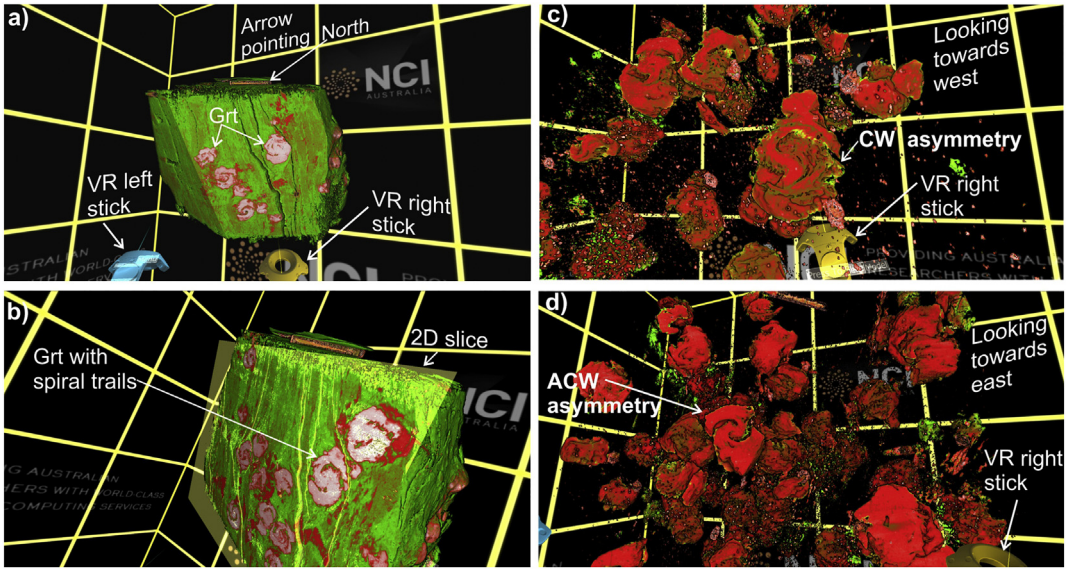

Fig. 3. (a, b) Images of the virtual-reality (VR) tour made inside the rock volume using a VR headset. Movements were controlled with the yellow and blue VR sticks visible in (a), (c) and (d). The sample can be cut and restored at any desired angle using the VR sticks. (c, d) When the rock matrix is rendered transparent, the user can immersed inside the rock volume to inspect the inclusion trail geometry. FIA can be obtained from any single or multiple sets of garnets. CW: clockwise, ACW: anticlockwise. (For interpretation of the references to colour in this figure legend, the reader is referred to the web version of this article).

vive.com/us/product/vive-pro/) and the open-source scientific visualization software 'Drishti' (https://github.com/nci/drishti). The VR allows one to 'walk around' inside the rock volume using the VR's control sticks (Fig. 3). The sample can be cut and restored on the spot at any desired angle and the FIA can be obtained from any single or multiple set of garnet porphyroblasts.

Using PerGeos, the rock matrix was rendered transparent to inspect the visual distribution of garnet porphyroblasts within the sample. 3D volume rendered image showed more or less even population of garnet porphyroblasts of different sizes (see below) with a relatively high proportion in the northwestern corner (Fig. 4a). This garnet-only visualization allows the best places for the 2D digital sections to be selected.

With the help of PerGeos 'clipping' tool, FIA can be determined in two ways. The first approach is the 'digital' version of the traditional method. The sample was dissected into 6 vertical digital sections at an interval of 30° starting from 360° (Fig. 4). Due to the non-destructive nature of the XCMT method, and unlike traditional thin sectioning approaches, the digital sections were placed interactively where a maximum number of well-preserved porphyroblasts were encountered (Fig. 4). Spiral inclusion trails were clearly observed in all digital sections, except for the one lying close to the FIA. Sections 360° to 060° show clockwise (CW) asymmetry of inclusion trails, whereas sections 120° and 150° exhibit anticlockwise (ACW) pattern (Fig. 4c). Section 090° shows closed inclusion trail patterns and asymmetric to symmetric geometries that are typically seen in sections cut close to the FIA (Johnson, 1993; Cihan, 2004).

The second way of measuring the FIA can be done without placing 6 or more fixed reference vertical digital sections. With the help of clipping tool, a digital vertical section can be placed anywhere in the rock volume and for visualization purposes, one side of the block can be removed (Fig. 4c). A double-up section can be interactively rotated 360° about a vertical axis, across the rock volume or through single porphyroblast with reference to the north to determine FIA. The latter case is especially suitable for inconsistences in the geometry of spiral trails in individual porphyroblasts in a single sample (cf. Bell et al., 1998).

3.2. High-resolution scan of a partial sample volume

The high-resolution scan of a partial sample volume is presented in Fig. 5 that allows the determination of minute inclusion trail details (Figs. 5 and 6). In addition to the set of vertical sections, a series of horizontal ones passing through porphyroblast centres were also studied (2 representative sections are shown in Fig. 5b–d). The horizontal sections, at least in this sample, do not show a clear dominant inclusion trail asymmetry and similar closed pattern as were seen in the N-090° striking vertical sections because the FIA plunges sub-horizontal (cf. Bell et al., 1995). The sample was further virtually cut in vertical sections striking N-080°, N-090°, N-100°, and N-110° to still better constrain the FIA trend. Section N-080° exhibited dominantly CW asymmetry and one or two garnets have closed inclusion trail patterns without a clear asymmetry. Section N-100° displayed a mixture of unclear spirals with closed patterns as well as ACW ones. Section N-110° clearly showed a dominant ACW asymmetry. Since section N-090° did not show any clear asymmetry, the FIA can be determined as N-090° with an estimated error of ±5° (Fig. 6).

4. Textural analysis

A series of vertical thin sections were cut perpendicular to the matrix foliation and the FIA axis from an underlying slab of the same sample (W-11). The one shown in Fig. 7a exhibits a representative garnet porphyroblast in addition to staurolite and kyanite porphyroblasts. The garnet porphyroblasts show a distinct core and rim, where quartz-rich inclusion trails in the core are surrounded by quartz-poor inclusion trails in the rim (Fig. 7a). The core-rim contrast can also been seen in the EMPA chemical map for Mn (Fig. 7b), but not on the Ca map (Fig. 7c). The shear sense, based on the geometry of spiral inclusion trails, can be interpreted as either ACW or CW (viewing west in the N–S section) depending on the rotation versus non-rotational porphyroblast models, respectively (Fig. 7d, e). Staurolite porphyroblasts preserve sigmoidal inclusion trails and show opposite asymmetry of inclusion trails compared to the garnet porphyroblasts.

5. Quantitative analysis

Porphyroblast shapes viewed in thin sections have been quantified by best-fit ellipses (Aerden and Sayab, 2017), whose principle axes generally do not have exactly the same length as the longest and shortest Feret diameters of the object. Hence, we preferred to characterize garnet porphyroblast shapes with the long (X_{GT}), medium (Y_{GT}), and short

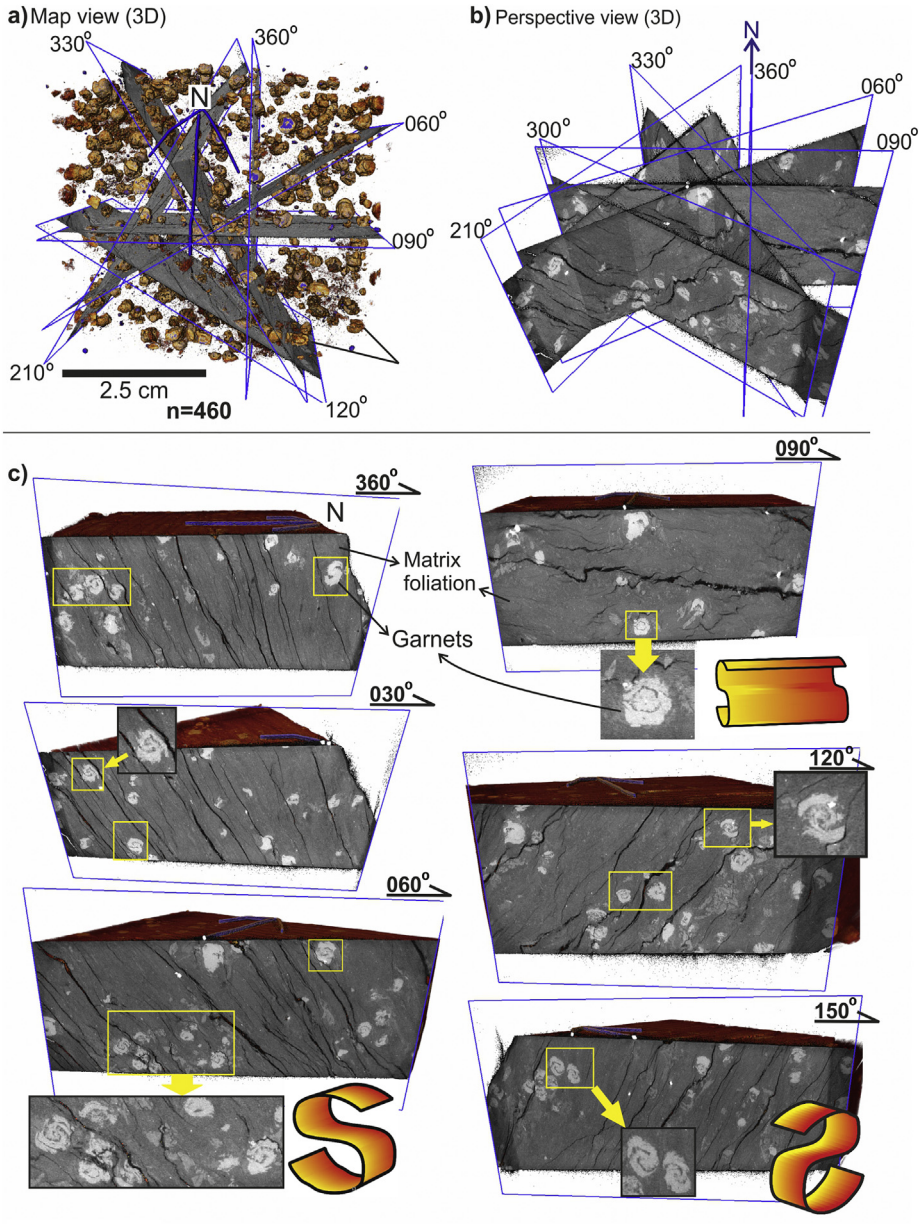

Fig. 4. (a) 3D XCMT image (map-view) of sample W-11 showing random distribution of garnet porphyroblasts in brown, whereas the rock matrix is rendered transparent. Six vertical slices striking 360°, 030°, 060°, 090°, 120° and 150° were selected in the rock volume to maximize the number of porphyroblasts in each section. The size of each section is the same as a standard thin section (2.5 cm × 5 cm), but digital slicing allows sections to crosscut each other, which is not possible with thin sections. (b) Perspective view of the same sections shown in (a). Garnets appear brighter in the matrix because of their higher density and hence X-ray attenuation. (c) Same slices as in (a) and (b) viewed head on showing clockwise curvature of 'S' shaped inclusion trails in sections 360° to 060° but anticlockwise curvature of 'Z' shaped inclusion trails in sections 120° to 150° can be observed. Section 090° exhibits closed patterns without clear asymmetry because it is sub-parallel to the average FIA orientation of porphyroblasts in the sample. (For interpretation of the references to colour in this figure legend, the reader is referred to the web version of this article).

(Z_{GT}) Feret diameters or axes (Fig. 7f). Close inspection of the shape of a garnet porphyroblast revealed that the X_{GT} axes may not necessarily perpendicular to the curvature axis of the inclusion trails, but it can be parallel to it (Fig. 8; Trouw et al., 2008).

Detailed segmentation procedures are described in, for example, Ketcham (2005) and Sayab et al. (2017) and only briefly outlined here. In-situ 3D quantitative analyses were performed on garnet porphyroblasts, in the full slab (cf. Figs. 2a and 4a), to estimate their volume, surface area, aspect ratio, spatial orientation, size and shape. Individual garnet porphyroblasts were separated from the rock matrix using the algorithm 'marker-based watershed' segmentation built-in PerGeos software. Volumes were calculated as the number of voxels in the outer layer of each garnet porphyroblast. Volume rendering of the whole sample, whereby the matrix is set as transparent, shows a more or less even population of garnet porphyroblasts suggesting that the sample is chemically heterogeneous. Although we counted 460 garnets in the sample (Fig. 4a), only 159 were selected for detailed quantitative analysis because the others either touch the boundaries of the scan or are broken and cracked. The total volume fraction of garnet in the sample estimated through full segmentation is ~4.5%.

The shape of garnet porphyroblasts is shown on a Flinn plot, and was estimated as ratios between the X_{GT} : Y_{GT}, and Y_{GT} : Z_{GT} Feret axes, respectively. The Flinn plot indicates that most garnets fall between prolate and oblate shapes (Fig. 9a) with an average aspect ratio (X_{GT}/Z_{GT}) of about 1.5 (Fig. 9b). The average mean volume and area of the garnet porphyroblasts is 9.1 mm^3 and 26 mm^2, respectively (Fig. 9c). The

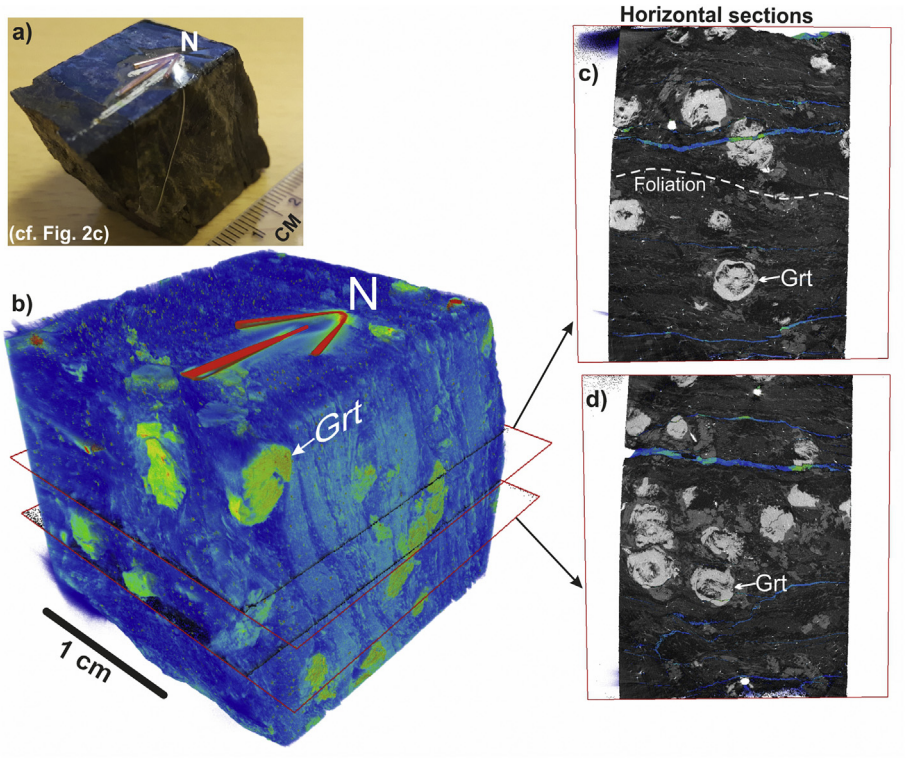

Fig. 5. (a) Partial sample (part of the same sample W-11) (cf. Fig. 2c). (b) Volume rendering of the sample as shown in (a). (c, d) Horizontal slices showing closed pattern of inclusion trails within garnet (Grt) porphyroblasts. Brass wire pointing North.

volume to area plot shows a positive relationship between the two parameters, whereas the volume to aspect ratio plot exhibits a slight inverse relationship between garnet volume and aspect ratio (Fig. 9b, c). Orientations of X_{GT} axes exhibit a broad E–W trend maximum followed by WNW–ESE and smaller NNE–SSW and NNW–SSE maxima (Fig. 9d), and quite variable plunges that cluster about a sub-vertical orientation maximum and a small sub-horizontal peak (Fig. 9e, f).

6. Discussion

6.1. Porphyroblast growth and non-rotation vs. rotation models

Zoned garnet porphyroblasts record continuous or punctuated tectonic histories and metamorphic processes spanning millions of years as revealed by direct Lu–Hf and Sm–Nd garnet geochronology or indirect monazite dating methods (Williams et al., 2007; Pollington and Baxter, 2010). Trouw et al. (2008) studied the shape and shape elongation of garnet porphyroblasts in sections cut perpendicular to the matrix foliation and parallel to the stretching lineation, but assumed that the longest dimension of garnet porphyroblasts was contained in these sections and that apparent porphyroblasts rotation axes are perpendicular to it. However, our data (Figs. 8 and 9f) show that long axes (X_{GT}) can have orientations ranging between perpendicular and parallel to the lineation (cf. Bell et al., 1997).

Garnet porphyroblasts in sample W-11 belong to a single FIA set as they have a consistent curvature sense except in sections lying very close to the E–W average FIA trend (Fig. 6). The main E–W maximum of X_{GT} axes in the rose diagram of Fig. 9d, parallel to the average FIA, is most likely controlled by the 3D shape of micro-lithons and the orientation of crenulation axes as sketched in Fig. 10 (cf. Bell, 1985; Aerden and Ruiz-Fuentes, 2020). Similarly, the WNW–ESE, NNE–SSW and NNW–SSE maxima indicate that the X_{GT} axes may not necessarily aligned parallel to the FIA. Besides a small sub-horizontal peak (Fig. 9e), the average orientation of porphyroblast X_{GT} axes in sample W-11 is sub-vertical and perpendicular to the FIA, something that is not explained by rotational models, but is as predicts by the non-rotation model. This model predicted sub-vertical and/or sub-horizontal preferred orientations of inclusion trails, which have been confirmed in different mountain belts (e.g. Hayward, 1992; Johnson, 1992; Aerden, 2004; Sayab, 2005; Aerden and Sayab, 2008; Kim and Sanislav, 2017). Recently, Aerden and Ruiz-Fuentes (2020) have shown that similar preferred orientations also affect the shape of porphyroblast crystals because they inherited the shape of low strain lenses in which they nucleate and grew. Considering the 'snowball' hypothesis of spiral inclusion trails, where porphyroblasts grow during uniaxial rotation relative to a single 'shear zone' foliation, one should rather expect porphyroblast X_{GT} axes to align with the rotation axes contrary to what is observed in Fig. 9f.

6.2. XCMT method and 3D fabric analysis

FIA studies show that two to three dozen samples are typically needed to correlate FIA orientations at the belt scale and regional structural analysis, which amounts to tedious preparation of hundreds of vertical and horizontal oriented thin sections in addition to carrying large samples in the field. In our experience, only about one third to half of all samples collected yield FIA as many samples are affected by reaction or replacement textures, retrogression, poorly developed inclusion trails, limited porphyroblasts or chemical weathering. XCMT significantly alleviates traditional thin-sectioning procedures and allows FIA to be determined on a relatively small rock specimen in a non-destructive way (Huddlestone-Holmes and Ketcham, 2010; Sayab et al., 2015). It illuminates the complete internal structure of a rock sample, which depends on the scanning resolution and contrast in mineral densities. 3D volume rendering of the sample allows to select the best plane(s) to be cut for thin sectioning or volumes for bulk chemical analysis. Hence, a large part of the sample can be preserved for further studies. In addition, 3D quantitative data of porphyroblasts permit study of sample-scale metamorphic processes, which can be used in the

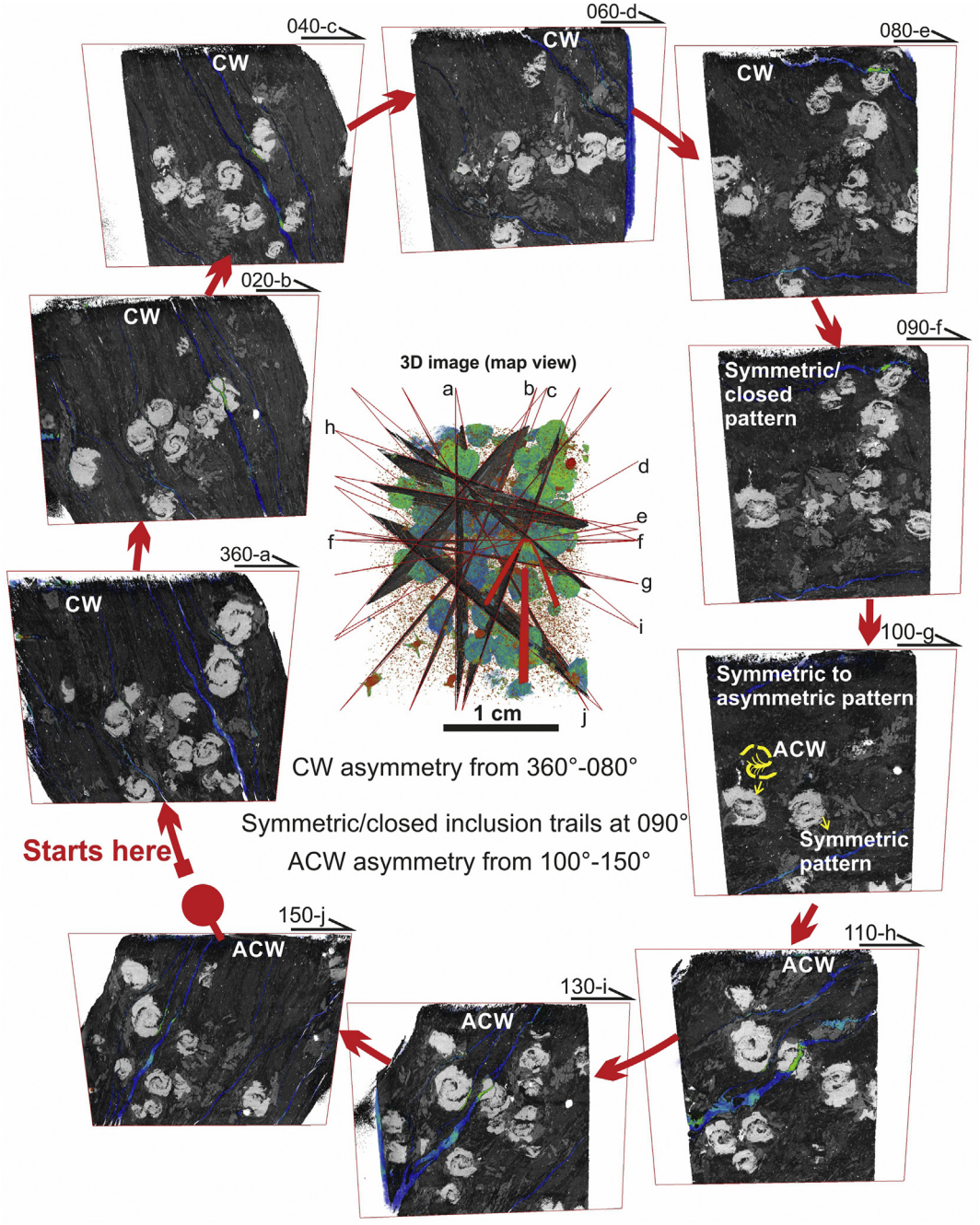

Fig. 6. Small sample piece of sample W-11 scanned at a higher resolution (12 μm) and dissected into closely spaced vertical slices, especially close to the FIA (N-080°, N-090°, N-100°, N-110°). Each vertical slice is labelled in an alphabetical order ('a' to 'j') next to the orientation mark and corresponding to the same vertical slices shown on the 3D image in the centre. CW: Clockwise, ACW: Anticlockwise.

understanding of regional tectonic analysis (e.g. Petley-Ragan et al., 2016; George et al., 2018; Corti et al., 2019). Overall, XCMT highlights a powerful technique for 3D microstructural analysis that complements traditional study of thin-sections and regional metamorphic history.

6.3. Regional tectonic implications

The E–W FIA orientation in the given sample (W-11) is consistent with the bulk horizontal N–S shortening of the India-Kohistan Island Arc-Asia collision (e.g. St-Onge et al., 2013; Treloar et al., 2019). The sample (W-11) came from the lower sillimanite zone of Palin et al. (2012), in the hanging wall of the Main Karakoram Thrust or Shyok Suture Zone, where three discrete metamorphic events (M0, M1, M2) of andalusite, sillimanite and kyanite grade have been reported and dated (Fraser et al., 2001; Palin et al., 2012). Based on the U–Pb dating of metamorphic monazites, preserved within garnet porphyroblast, these events were dated at 105.5 ± 0.8 Ma, 44.0 ± 2.0 Ma and 28.2 ± 0.8 Ma, respectively, from a single sample and linked to intrusion of the Karakoram Batholith during early subduction of the Tethys Ocean (M0), followed by accretion and collision of the Kohistan Island Arc with the Asian margin (M1) and subsequent crustal thickening stages (M2). A younger staurolite-grade metamorphic event (M3) was dated at 16.0 ± 1.0 Ma in the southern parts of the Hunza Valley, south of the Hasanabad thrust (Fraser et al., 2001).

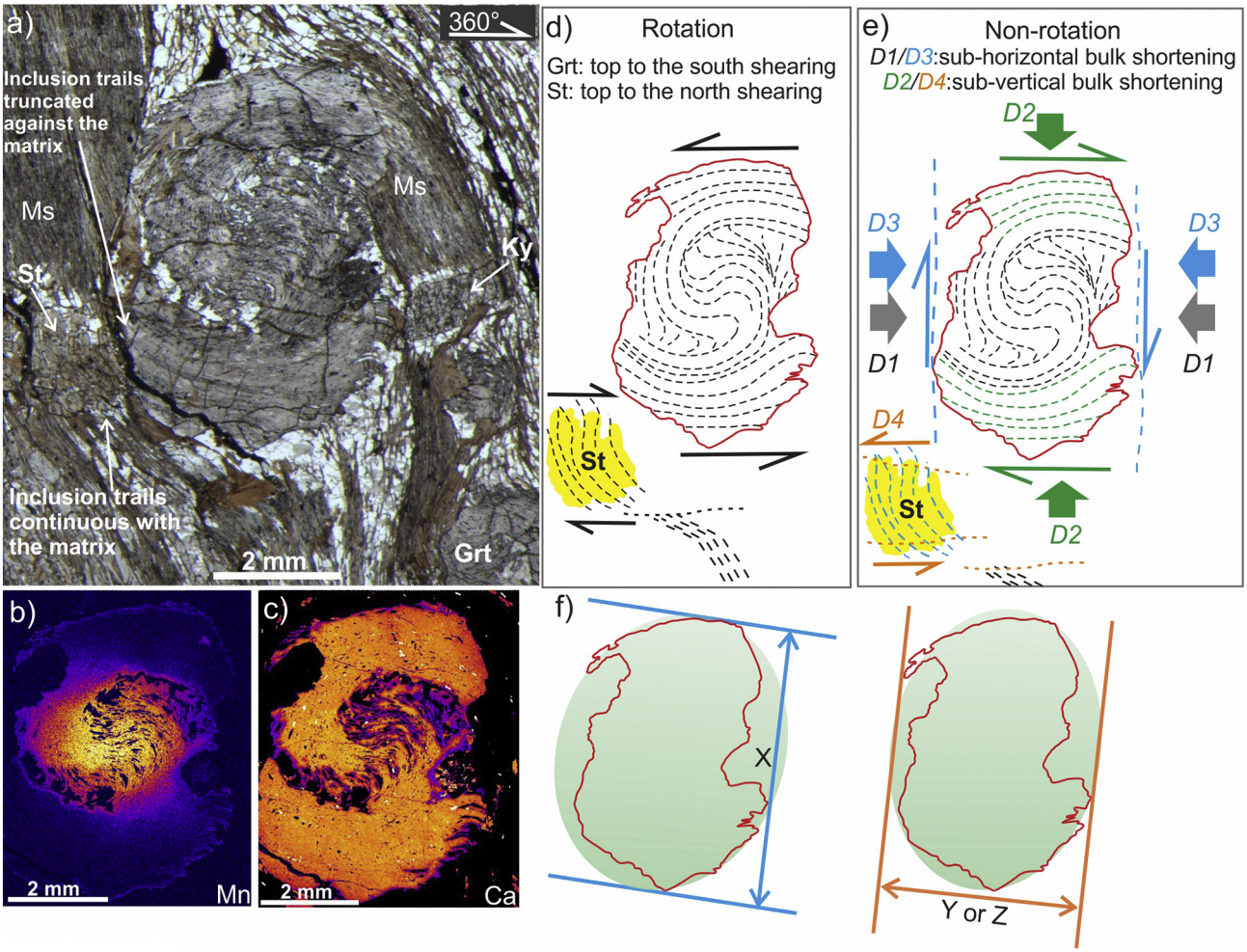

Fig. 7. (a) Photomicrograph of garnet porphyroblast in a vertical section of sample W-11 oriented normal to its FIA (PPL). Note relatively small kyanite (Ky) and staurolite (St) porphyroblasts on the lower sides of the large garnet porphyroblast. Inclusion trails in the garnet porphyroblast curve from gently- to steeply-dipping in the core to sub-horizontal in the rim. (b, c) Mn and Ca element maps of the garnet shown in (a). (d, e) Sketch of the porphyroblast in (a) interpreting the shear sense (d) or shear-sense history (e) according to the rotation vs. the non-rotation model. The different orientations of inclusion trail foliations and associated deformation events (in different colours) implied by the non-rotation can be linked to the metamorphic path of the rock as discussed in the body text and Fig. 12. Note, staurolite porphyroblast hosts inclusion trails with opposite shear sense as compared to the garnet. (f) Feret's long (X) and medium (Y) or short (Z) axes.

Porphyroblasts grow over a pre-existing foliation early during the crenulation development and ceases as cleavage begins to develop against its rims (e.g. Bell, 1985; Shah et al., 2012; Bell and Fay, 2016). Thus, the foliation(s) preserved within the porphyroblast pre-dates the matrix foliation. Sample W-11 preserves garnet porphyroblasts showing successive sub-horizontal and sub-vertical inclusion trail

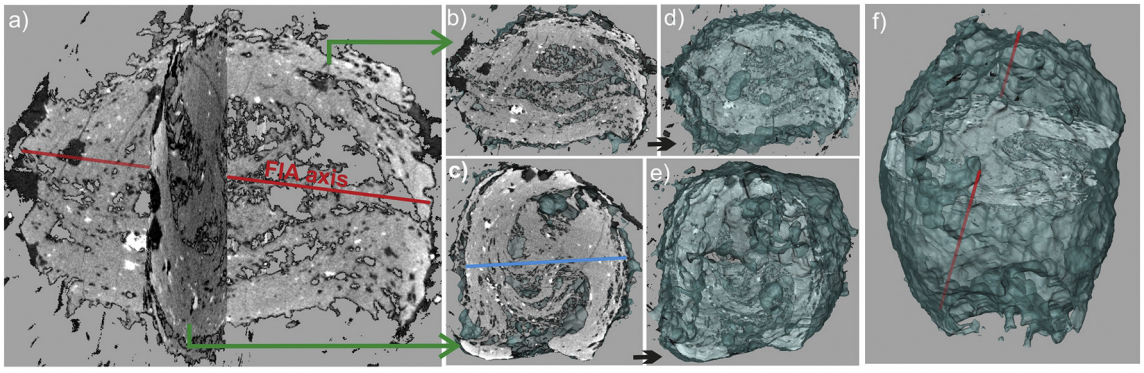

Fig. 8. Different 3D representations of a single garnet porphyroblast in sample W-11. Resolution of the scan is 5 μm. (a) Two vertical slices along and across the FIA (slices are perpendicular to each other and shown with different brightness). The longest dimension (3.69 mm) of the garnet is sub-parallel to its FIA (red line). (b, c) Same orthogonal vertical slices striking N-090° and N-360° in (b) and (c), respectively, showing the cross-sectional geometry of inclusion trails. The shortest dimension measures 2.66 mm (blue line). (d, e) 3D volume renderings highlighting the outer surface of the garnet in light green. Grey colour 2D slices, same as in (b) and (c), inside the garnet are for 3D visualization purposes. (f) 3D perspective view showing the FIA and long axis in red. (For interpretation of the references to colour in this figure legend, the reader is referred to the web version of this article).

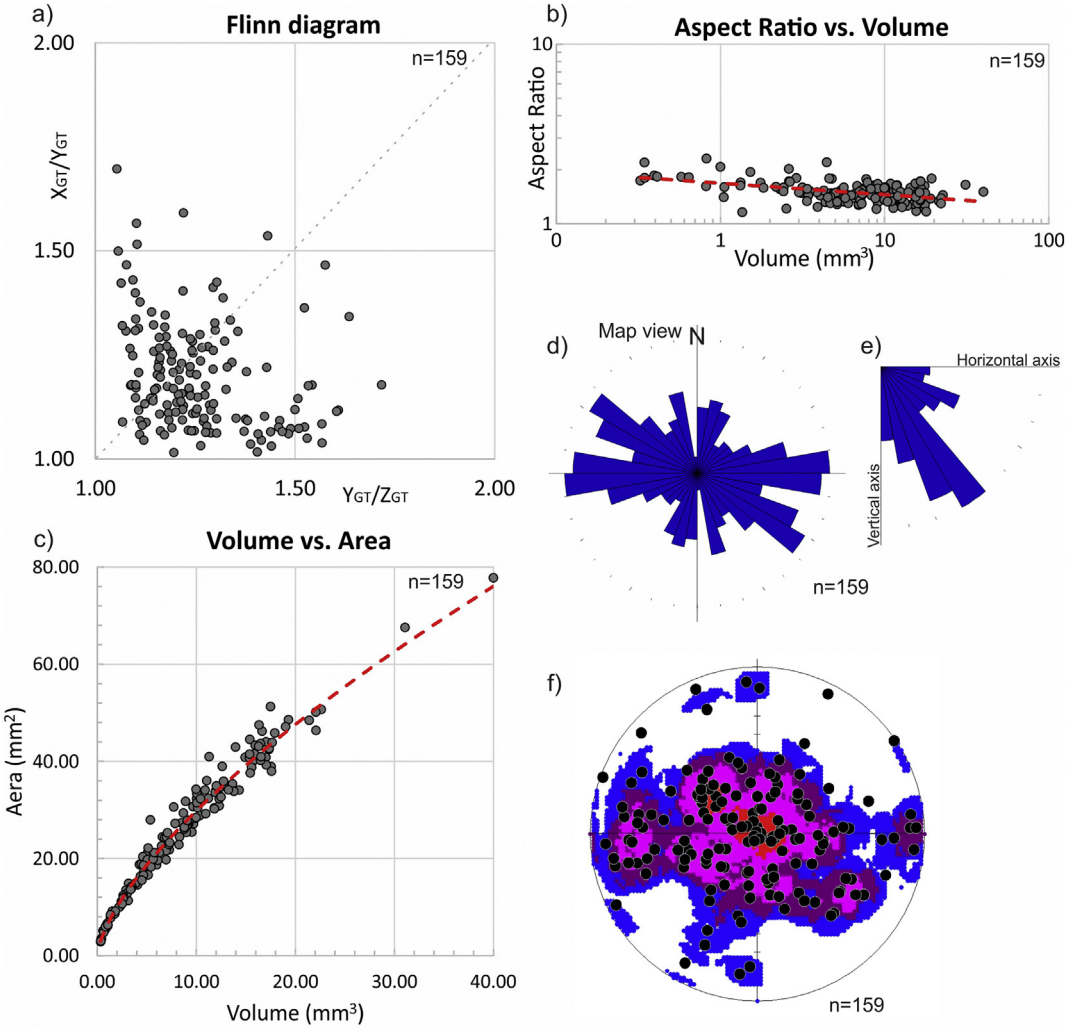

Fig. 9. 3D quantitative data for garnet porphyroblasts in sample W-11. (a) Flinn diagram for maximum (X_{GT}), intermediate (Y_{GT}) and minimum (Z_{GT}) Feret axes of the studied garnets showing the presence of both prolate and oblate grain shapes. (b) Aspect ratio (X_{GT}/Z_{GT}) vs. volume plot showing a linear trend between logarithms of grain volume and aspect ratio, where volume increases with a slight decrease in the aspect ratio. Mean aspect ratio (~1.5) suggest low to moderate gain-shape anisotropy. (c) Area vs. grain volume plot showing volume is directly proportional to the area. (d) Rose plot showing preferred E–W and WNW–ESE trends of garnet long axes (X_{GT}), whereas some smaller peaks close to the N–S orientation. (e) Plunge angles of the garnet long axes (X_{GT}). (f) The contour pattern in the stereoplot shows a broad sub-vertical maximum of the long axes (X_{GT}) surrounded by shallow orientations as can also be seen in 'e'. (For interpretation of the references to colour in this figure legend, the reader is referred to the web version of this article).

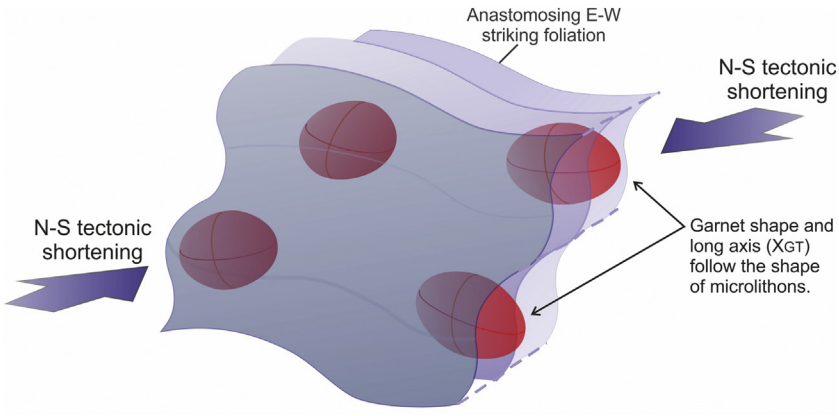

Fig. 10. Conceptual model showing that the shape of garnet porphyroblasts is controlled by the low-strain domains surrounded by broadly E–W striking anastomosing foliation. Because of the anastomosing pattern prior to the garnet growth, the orientation of the long axis (X) of the garnet porphyroblasts vary from one domain to another.

foliations in the core and sub-horizontal inclusion trails in the rim, respectively (Fig. 11a–c), wherein the FIA is controlled by the strike of the intermediate sub-vertical inclusion trail foliation (Fig. 11c). We did not find petrographic evidence that allowed determination of whether the garnet cores in sample W-11 grew during the initial andalusite-grade metamorphism (M0) or the subsequent sillimanite grade overprint (M1). Textural relationships suggest that both kyanite and staurolite porphyroblasts grew over the steeply-dipping matrix foliation after garnet growth had ceased (Fig. 11). This textural relationship affirms that the final stage of garnet growth (stage-III) was a result of prograde metamorphism and bulk horizontal shortening that produced a sub-vertical foliation plane against garnet rims, while in the matrix a pre-existing foliation was reactivated and steepened (Fig. 12a–d).

Garnet growth stage-II was associated with gravity-induced sub-vertical shortening and horizontal foliation development, that interrupted crustal shortening and vertical foliation development during stage-I and -III. However, we do not know if it was this gravitational collapse event that caused the major decompression that led to sillimanite growth in the area or whether that decompression occurred before the growth of our stage II garnets. Although, peak sillimanite grade metamorphism has been assigned at 44.0 ± 2.0 Ma in the Hunza Valley (U–Pb monazite ages by Fraser et al., 2001), emplacement of monzogranite and leucogranite dykes, intruded into the Karakoram batholith between 52 and 50 Ma (U–Pb zircon by Fraser et al., 2001), could explain the commencement of this decompression phase. The timing of peak sillimanite grade metamorphism in the Hunza Valley is within the error range of the 42 Ma E–W trending FIA 4 of Bell and Sapkota (2012) from the Central Himalayas. We interpret that the E–W FIA in the sample W-11 is equivalent to FIA 4 of Bell and Sapkota (2012).

The core of the garnet shows sub-horizontal to sub-vertical inclusion trail pattern, which can be interpreted to result from the initial collision after the andalusite-grade contact metamorphism (M0 of Palin et al., 2012) with the closure of the Shyok Suture Zone at 82 Ma (Foster et al., 2004). The latter age is based on the U–Pb dating of monazite inclusions within garnet cores from the sillimanite zone of the Hunza Valley and might be equivalent to the pre-existing sub-horizontal foliation trapped within the garnet cores of sample W-11 (Fig. 11a–c). We have not found any datable size monazites in the garnet. Core to rim micro-sampling of garnet porphyroblasts for Sm–Nd geochronological investigation is required to confirm the different phases of garnet growth versus metamorphic episodes (Pollington and Baxter, 2010).

Fig. 12a–d schematically shows the development of three near-orthogonal foliations trapped within garnet porphyroblasts in response to (at least) three folding events with a consistent CW shear sense, while looking west in the N–S section. However, staurolite porphyroblasts show sigmoidal inclusion trail patterns with an ACW shear sense. Bell and Sapkota (2012) reported a dominantly CW shear sense in garnet porphyroblasts hosting FIAs 1–4 in the hanging wall of the Main Central Thrust in the Central Himalayas, but an ACW shear sense dominated the late deformation history associated with FIA 5. The dramatic change in shear sense, between FIA 4 and 5, has been attributed to the progressive northward roll-on of the orogen core below the basal decollement, which caused top-to-the-south shear above the decollement surface. Consequently, the samples sitting above the basal decollement extruded to the south with top-to-the south shear sense exhuming the rock package to the surface (figs. 7 and 8 of Bell and Sapkota, 2012).

The remarkable similarity of the change in shear sense from ACW to CW on the hanging wall of the suture zones across the Himalayan belt implies that the sample W-11 followed the same deformation paths as reported from the Central Himalayas (Bell and Sapkota, 2012) and shown in Fig. 12e–h. Peak kyanite-grade metamorphic pressure in the Hunza Valley is estimated around 7.8 kbar at 28.2 ± 0.8 Ma (Palin et al., 2012), whereas garnet core pressure (P) and temperature (T) are estimated at 6 kbar and 553 ± 23 °C around 82 Ma (Foster et al., 2004), suggesting that the garnet cores were formed somewhere around 20 to 21 km of depth (Fig. 12a). These P-T estimates along with the CW shear sense in garnet porphyroblasts indicate the location of the sample within the orogen (Fig. 12e–h). As the age of staurolite-grade metamorphism is 16 Ma in the Hunza valley (Fraser et al., 2001), then the switch in the shear sense from CW, in the garnet, to ACW, in the staurolite, while looking west in the N–S section, occurred just before or around this time as a result of progressive roll-on tectonics below the basal decollement (Bell and Newman, 2006). The model shown in Fig. 12e–h might have gone through several intermittent stages of upright folding and gravity-induced nappe formations and associated sub-vertical and sub-horizontal foliation development, respectively, however, we have only shown the main stages for simplicity. This is consistent with the multiple metamorphic stages of the southern Karakorum margin where repeated stages of upright folding, nappe and dome formation, exhumation and sporadic crystallization ages of intrusions at 52–50 Ma, 35 ± 1.0 Ma, 25 to 13 Ma, and 9.3 ± 0.2 Ma were reported (Fraser

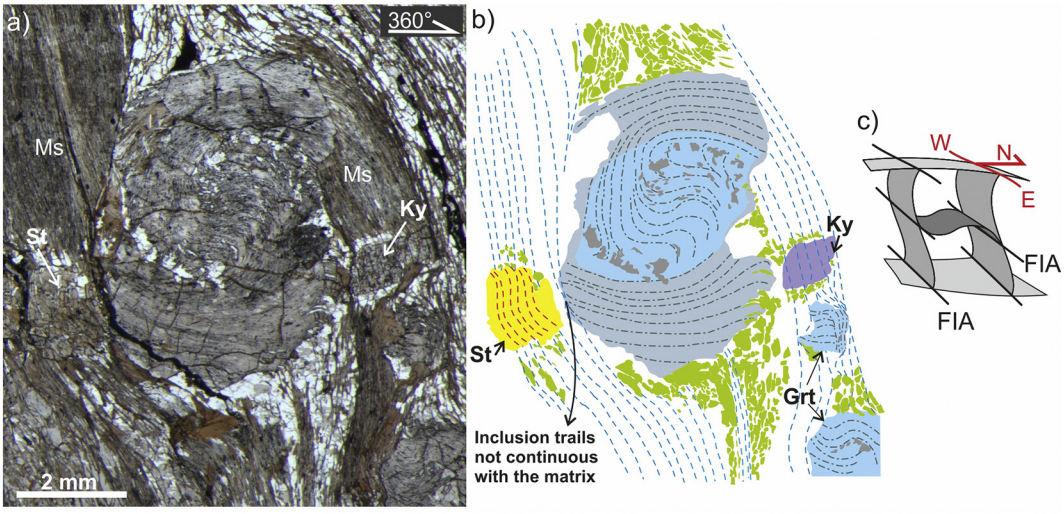

Fig. 11. (a) Photomicrograph, corresponding sketch (b) and FIA trend (c) of a representative spiral garnet in sample W-11. Note contrasting inclusion asymmetries in the garnet (CW) and staurolite (ACW) porphyroblasts and explained in Fig. 12. Grt: garnet, Ky: kyanite, St: staurolite, Ms: muscovite.

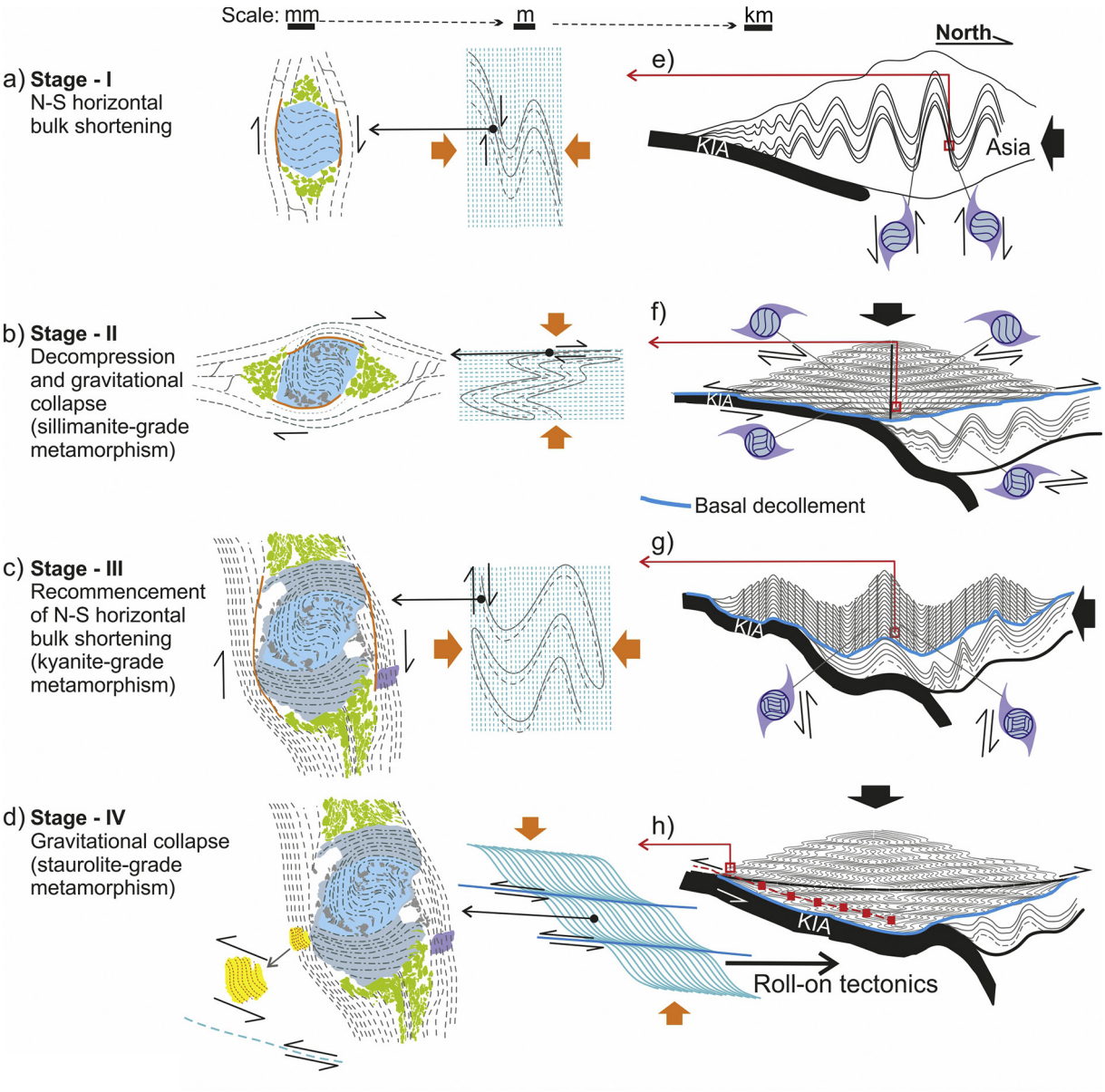

Fig. 12. (a–d) Tectonic evolution of the garnet, kyanite and staurolite porphyroblasts in the context of the kinematic evolution of the Hunza Valley of the KMC, which is further interpreted in (e) to (h) at the orogen scale. Garnet grew in crenulation hinges during the first N–S horizontal bulk shortening stage (I) of deformation that produced a sub-vertical foliation. Stage I occurred post andalusite-grade metamorphism (M0) of Palin et al. (2012), plausibly after 82 Ma (Foster et al., 2004). Gravitational collapse stage (II) was accompanied by decompression, and might have associated with the sillimanite-grade metamorphism (44 ± 2.0 Ma), where the garnet grew over a steeply-pitching foliation that formed during stage I. Renewed N–S horizontal bulk shortening stage (III) created a new sub-vertical oriented foliation, where the garnet grew over sub-horizontal foliation developed during the stage II. Both kyanite and staurolite in the matrix must have formed after the garnet growth as independently dated at 28.2 ± 0.8 Ma and 16 ± 1.0 Ma, respectively (see text for the discussion). Each garnet growth phase is associated with the folding event, which can be explained with the crustal-scale kinematic models (e–h) presented by Bell and Newman (2006) and Bell and Sapkota (2012). The key role of roll-on tectonics below the basal decollement is highlighted, where the rocks above it pushed towards the south and extruded to the surface (shown in 'h' as red squares) as a result of gravity-induced thrusting. Ky: kyanite, St: staurolite, Ms: muscovite, KIA: Kohistan Island Arc. (For interpretation of the references to colour in this figure legend, the reader is referred to the web version of this article).

et al., 2001; Foster et al., 2004; Rolland et al., 2006; Searle et al., 2010; Palin et al., 2012; Searle and Hacker, 2019).

7. Conclusions

(1) XCMT-based virtual petrography is an in-situ, non-destructive, 3D visualization method that allows the determination of FIA in garnet porphyroblasts with spiral inclusion trails in a relatively large oriented sample in an efficient manner. FIAs can be measured with or without placing fixed digital sections across the whole sample or a single porphyroblast. The technique is especially useful if two to three dozen samples are planned for FIA analyses and micro-textural correlations across any given metamorphic belt.

(2) 3D quantitative data from porphyroblasts can be used in combination with the FIA orientation and EPMA chemical images to decipher porphyroblast growth and shape.

(3) The garnet long axis (X_{GT}) multimodal orientation data suggest that they inherit the shape of microlithons, and are independent of the rotation axis (or FIA) and favor the non-rotation porphyroblast model.

(4) The E–W FIA obtained from sample W-11 is consistent with the regional E–W striking foliation of the Hunza Valley of the KMC and depicts the India-Kohistan Island Arc-Asia collision. Based on the E–W orientation and CW shear sense along the inclusion trail foliations, the FIA can be correlated with FIA 4 of Central Himalayas obtained by Bell and Sapkota (2012). The inclusion trail pattern in the core and rim regions of the garnet porphyroblast along with kyanite in the steeply-dipping matrix foliation appears to be in accord with the episodic metamorphic evolution of the Hunza Valley from post-andalusite to kyanite via sillimanite, established previously by Fraser et al. (2001) and Palin et al. (2012). The switch in the asymmetry from CW to ACW in the garnet and staurolite porphyroblasts, respectively, while looking west, shed light on the key role of orogen-scale roll-on tectonics.

Declaration of Competing Interest

The authors declare that they have no known competing financial interests or personal relationships that could have appeared to influence the work reported in this paper.

Acknowledgements

We thank Pentti Hölttä and Syed Zahid Shah for many useful discussions. We thank the referees, F. George and an anonymous reviewer, for their constructive comments.

References

Aerden, D., 2003. Preferred orientation of Planar microstructures determined via statistical best-fit of measured intersection-lines: the "FitPitch" computer program. J. Struct. Geol. 25, 923–934. https://doi.org/10.1016/S0191-8141(02)00119-0.

Aerden, D., 2004. Correlating deformation in Variscan NW-Iberia using porphyroblasts; implications for the Ibero-Armorican Arc. J. Struct. Geol. 26, 177–196. https://doi.org/10.1016/S0191-8141(03)00070-1.

Aerden, D., Ruiz-Fuentes, A., 2020. X-ray computed micro-tomography of spiral garnets: a new test of how they form. J. Struct. Geol., 104054 https://doi.org/10.1016/j.jsg.2020.104054.

Aerden, D., Sayab, M., 2008. From Adria- to Africa-driven orogenesis: evidence from porphyroblasts in the Betic Cordillera, Spain. J. Struct. Geol. 30, 1272–1287.

Aerden, D., Sayab, M., 2017. Probing the prodigious strain fringes from Lourdes. J. Struct. Geol. 105, 88–106. https://doi.org/10.1016/j.jsg.2017.11.001.

Aerden, D., Bell, T.H., Puga, E., Sayab, M., Lozano, J.A., Diaz de Federico, A., 2013. Multi-stage mountain building vs. relative plate motions in the Betic Cordillera deduced from integrated microstructural and petrological analysis of porphyroblast inclusion trails. Tectonophysics 587, 188–206. https://doi.org/10.1016/j.tecto.2012.11.025.

Aerden, D.G.A.M., 1995. Porphyroblast non-rotation during crustal extension in the Variscan Lys-Caillaouas Massif, Pyrenees. J. Struct. Geol. 17, 709–725. https://doi.org/10.1016/0191-8141(94)00090-M.

Bell, T.H., 1985. Deformation partitioning and porphyroblast rotation in meta-morphic rocks: a radical reinterpretation. J. Metamorph. Geol. 3, 109–118. https://doi.org/10.1111/j.1525-1314.1985.tb00309.x.

Bell, T.H., Fay, C., 2016. Holistic microstructural techniques reveal synchronous and alternating andalusite and staurolite growth during three tectonic events resulted from shifting partitioning of growth vs deformation. Lithos 262, 699–712. https://doi.org/10.1016/j.lithos.2016.06.031.

Bell, T.H., Johnson, S.E., 1989. Porphyroblast inclusion trails: the key to orogenesis. J. Metamorph. Geol. 7, 279–310. https://doi.org/10.1111/j.1525-1314.1989.tb00598.x.

Bell, T.H., Newman, R., 2006. Appalachian orogenesis: the role of repeated gravitational collapse. Spec. Pap. Geol. Soc. Am. 414, 95–118. https://doi.org/10.1130/2006.2414(06).

Bell, T.H., Sanislav, I.V., 2011. A deformation partitioning approach to resolving the sequence of fold events and the orientations in which they formed across multiply deformed large-scale regions. J. Struct. Geol. 33, 1206–1217. https://doi.org/10.1016/j.jsg.2011.03.014.

Bell, T.H., Sapkota, J., 2012. Episodic gravitational collapse and migration of the mountain chain during orogenic roll-on in the Himalayas. J. Metamorph. Geol. 30, 651–666. https://doi.org/10.1111/j.1525-1314.2012.00992.x.

Bell, T.H., Welch, P.W., 2002. Prolonged Acadian orogenesis: Revelations from foliation intersection axis (FIA) controlled monazite dating of foliations in porphyroblasts and matrix. Am. J. Sci. 302, 549–581.

Bell, T.H., Rubenach, M.J., Fleming, P.D., 1986. Porphyroblast nucleation, growth and dissolution in regional metamorphic rocks as a function of deformation partitioning during foliation development. J. Metamorph. Geol. 4, 37–67. https://doi.org/10.1111/j.1525-1314.1986.tb00337.x.

Bell, T.H., Forde, A., Hayward, N., 1992. Do smoothly curving, spiral-shaped inclusion trails signify porphyroblast rotation? Geology 20, 59–62.

Bell, T.H., Forde, A., Wang, J., 1995. A new indicator of movement direction during orogenesis: measurement technique and application to the Alps. Terra Nova 7, 500–508. https://doi.org/10.1111/j.1365-3121.1995.tb00551.x.

Bell, T.H., Hickey, K.A., Wang, J., 1997. Spiral and staircase inclusion trail axes within garnet and staurolite porphyroblasts from schists of the Bolton Syncline, Connecticut: timing of porphyroblast growth and the effects of fold development. J. Metamorph. Geol. 15, 467–478. https://doi.org/10.1111/j.1525-1314.1997.00032.x.

Bell, T.H., Hickey, K.A., Upton, J.G., 1998. Distinguishing and correlating multiple phases of metamorphism across a multiply deformed region using the axes of spiral, staircase and sigmoidal inclusion trails in garnet. J. Metamorph. Geol. 16, 767–794.

Cihan, M., 2004. The drawbacks of sectioning rocks relative to fabric orientations in the matrix: a case study from the Robertson River Metamorphics (Northern Queensland, Australia). J. Struct. Geol. 26, 2157–2174. https://doi.org/10.1016/j.jsg.2004.07.001.

Cihan, M., Evins, P., Lisowiec, N., Blake, K., 2006. Time constraints on deformation and metamorphism from EPMA dating of monazite in the Proterozoic Robertson River Metamorphics, NE Australia. Precambrian Res. 145, 1–23. https://doi.org/10.1016/j.precamres.2005.11.009.

Cnudde, V., Boone, M.N., 2013. High-resolution X-ray computed tomography in geosciences: a review of the current technology and applications. Earth Sci. Rev. 123, 1–17. https://doi.org/10.1016/j.earscirev.2013.04.003.

Corti, L., Zucali, M., Visalli, R., Mancini, L., Sayab, M., 2019. Integrating X-Ray computed tomography with chemical imaging to quantify mineral re-crystallization from granulite to eclogite metamorphism in the Western Italian Alps (Sesia-Lanzo Zone). Front. Earth Sci. 7, 1–24. https://doi.org/10.3389/feart.2019.00327.

Dixon, J.M., 1976. Apparent "double rotation" of porphyroblasts during a single progressive deformation. Tectonophysics 34, 101–115.

Foster, G., Parrish, R.R., Horstwood, M.S.A., Chenery, S., Pyle, J., Gibson, H.D., 2004. The generation of prograde P-T-t points and paths; a textural, compositional, and chronological study of metamorphic monazite. Earth Planet. Sci. Lett. 228, 125–142. https://doi.org/10.1016/j.epsl.2004.09.024.

Fraser, J.E., Searle, M.P., Parrish, R.R., Noble, S.R., 2001. Chronology of deformation, metamorphism, and magmatism in the southern Karakoram Mountains. Bull. Geol. Soc. Am. 113, 1443–1455. https://doi.org/10.1130/0016-7606(2001)113<1443:CODMAM>2.0.CO;2.

Fusseis, F., Xiao, X., Schrank, C., De Carlo, F., 2014. A brief guide to synchrotron radiation-based microtomography in (structural) geology and rock mechanics. J. Struct. Geol. 65, 1–16. https://doi.org/10.1016/j.jsg.2014.02.005.

George, F.R., Gaidies, F., 2017. Characterisation of a garnet population from the Sikkim Himalaya: insights into the rates and mechanisms of porphyroblast crystallisation. Contrib. Mineral. Petrol. 172, 1–22. https://doi.org/10.1007/s00410-017-1372-y.

George, F.R., Gaidies, F., Boucher, B., 2018. Population-wide garnet growth zoning revealed by LA-ICP-MS mapping: implications for trace element equilibration and syn-kinematic deformation during crystallisation. Contrib. Mineral. Petrol. 173, 1–22. https://doi.org/10.1007/s00410-018-1503-0.

Ham, A.P., Bell, T.H., 2004. Recycling of foliations during folding. J. Struct. Geol. 26, 1989–2009. https://doi.org/10.1016/j.jsg.2004.04.003.

Hanna, R.D., Ketcham, R.A., 2017. X-ray computed tomography of planetary materials: a primer and review of recent studies. Chemie der Erde Geochem. 77, 547–572. https://doi.org/10.1016/j.chemer.2017.01.006.

Hayward, N., 1990. Determination of early fold axis orientations in multiply deformed rocks using porphyroblast inclusion trails. Tectonophysics 179, 353–369. https://doi.org/10.1016/0040-1951(90)90301-N.

Hayward, N., 1992. Microstructural analysis of the classical spiral garnet porphyroblasts of south-East Vermont: evidence for non-rotation. J. Metamorph. Geol. 10, 567–587.

Huddlestone-Holmes, C.R., Ketcham, R.A., 2010. An X-ray computed tomography study of inclusion trail orientations in multiple porphyroblasts from a single sample. Tectonophysics 480, 305–320. https://doi.org/10.1016/j.tecto.2009.10.021.

Jiang, D., Williams, P.F., 2004. Reference Frame, Angular Momentum, and Porphyroblast Rotation. 26, pp. 2211–2224. https://doi.org/10.1016/j.jsg.2004.06.012.

Johnson, S.E., 1992. Sequential porphyroblast growth during progressive deformation and low-P high-T (LPHT) metamorphism, Cooma complex, Australia: the use of microstructural analysis to better understand deformation and metamorphic histories. Tectonophysics 214, 311–339. https://doi.org/10.1016/0040-1951(92)90204-J.

Johnson, S.E., 1993. Testing models for the development of spiral-shaped inclusion trails in garnet porphyroblasts: to rotate or not to rotate, that is the question. J. Metamorph. Geol. 11, 635–659.

Ketcham, R.A., 2005. Three-dimensional grain fabric measurements using high-resolution X-ray computed tomography. J. Struct. Geol. 27, 1217–1228. https://doi.org/10.1016/j.jsg.2005.02.006.

Kim, H.S., Bell, T.H., 2005. Combining compositional zoning and foliation intersection axes (FIAs) in garnet to quantitatively determine early P-T-t paths in multiply deformed and metamorphosed schists: North Central Massachusetts, USA. Contrib. Mineral. Petrol. 149, 141–163. https://doi.org/10.1007/s00410-004-0640-9.

Kim, H.S., Sanislav, I.V., 2017. Foliation intersection/inflection axes within porphyroblasts (FIAs): a review of advanced applications and significance. Geosci. J. 21, 1013–1032. https://doi.org/10.1007/s12303-017-0047-z.

Palin, R.M., Searle, M.P., Waters, D.J., Horstwood, M.S.A., Parrish, R.R., 2012. Combined thermobarometry and geochronology of peraluminous metapelites from the Karakoram metamorphic complex, North Pakistan; New insight into the tectonothermal evolution of the Baltoro and Hunza Valley regions. J. Metamorph. Geol. 30, 793–820. https://doi.org/10.1111/j.1525-1314.2012.00999.x.

Passchier, C.W., Trouw, R.A.J., Zwart, H.J., Vissers, R.L.M., 1992. Porphyrolast rotation: eppur si muove*? J. Metamorph. Geol. 10, 283–294.

Patriat, P., Achache, J., 1984. India-Eurasia collision chronology has implications for crustal shortening and driving mechanism of plates. Nature 311, 615–621. https://doi.org/10.1038/311615a0.

Petley-Ragan, A., Gaidies, F., Pattison, D.R.M., 2016. A statistical analysis of the distribution of cordierite and biotite in hornfels from the Bugaboo contact aureole: implications for the kinetics of porphyroblast crystallization. J. Metamorph. Geol. 34, 85–101. https://doi.org/10.1111/jmg.12172.

Pollington, A.D., Baxter, E.F., 2010. High resolution Sm-Nd garnet geochronology reveals the uneven pace of tectonometamorphic processes. Earth Planet. Sci. Lett. 293, 63–71. https://doi.org/10.1016/j.epsl.2010.02.019.

Powell, C.M.A., Vernon, R.H., 1979. Growth and rotation history of garnet porphyroblasts with inclusion spirals in a Karakoram Schist. Tectonophysics 54, 25–43. https://doi.org/10.1016/0040-1951(79)90110-0.

Robyr, M., Carlson, W.D., Passchier, C., Vonlanthen, P., 2009. Microstructural, chemical and textural records during growth of snowball garnet. J. Metamorph. Geol. 27, 423–437. https://doi.org/10.1111/j.1525-1314.2009.00824.x.

Rolland, Y., Carrio-Schaffhauser, E., Sheppard, S.M.F., Pêcher, A., Esclauze, L., 2006. Metamorphic zoning and geodynamic evolution of an inverted crustal section (Karakorum margin, N Pakistan), evidence for two metamorphic events. Int. J. Earth Sci. 95, 288–305. https://doi.org/10.1007/s00531-005-0026-x.

Rosenfeld, J.L., 1970. Rotated Garnets in Metamorphic Rocks. Geological Society of America Special Paper, p. 129.

Sanislav, I.V., 2011. A long-lived metdatingamorphic history in the contact aureole of the Mooselookmeguntic pluton revealed by in situ of monazite grains preserved as inclusions in staurolite porphyroblasts. J. Metamorph. Geol. 29, 251–273. https://doi.org/10.1111/j.1525-1314.2010.00916.x.

Sayab, M., 2005. Microstructural evidence for N-S shortening in the Mount Isa Inlier (NW Queensland, Australia): the preservation of early W-E-trending foliations in porphyroblasts revealed by independent 3D measurement techniques. J. Struct. Geol. 27, 1445–1468. https://doi.org/10.1016/j.jsg.2005.01.013.

Sayab, M., 2006. Decompression through clockwise P-T path: implications for early N-S shortening orogenesis in the mesoproterozoic Mt Isa Inlier (NE Australia). J. Metamorph. Geol. 24, 89–105.

Sayab, M., 2008. Correlating multiple deformation events across the Mesoproterozoic NE Australia using foliation intersection axes (FIA) preserved within porphyroblasts. Gondwana Res. 13, 331–351.

Sayab, M., Suuronen, J.-P., Hölttä, P., Aerden, D., Lahtinen, R., Kallonen, A., 2015. High-resolution X-ray computed microtomography: a holistic approach to metamorphic fabric analyses. Geology 43, 55–58. https://doi.org/10.1130/G36250.1.

Sayab, M., Shah, S.Z., Aerden, D., 2016. Metamorphic record of the NW Himalayan orogeny between the Indian plate-Kohistan Ladakh Arc and Asia: revelations from foliation intersection axis (FIA) controlled P-T-t-d paths. Tectonophysics 671, 110–126. https://doi.org/10.1016/j.tecto.2015.12.032.

Sayab, M., Miettinen, A., Aerden, D., Karell, F., 2017. Orthogonal switching of AMS axes during type-2 fold interference: Insights from integrated X-ray computed tomography, AMS and 3D petrography. J. Struct. Geol. 103, 1–16. https://doi.org/10.1016/j.jsg.2017.09.002.

Schoneveld, C., 1977. A study of some typical inclusion patterns in strongly paracrystalline-rotated garnets. Tectonophysics 39, 453–471. https://doi.org/10.1016/0040-1951(77)90109-3.

Searle, M.P., 1991. Geology and Tectonics of the Karakoram Mountains. John Wiley and Sons, New York.

Searle, M.P., Hacker, B.R., 2019. Structural and metamorphic evolution of the Karakoram and Pamir following India–Kohistan–Asia collision. Geol. Soc. Lond., Spec. Publ. 483, 555–582. https://doi.org/10.1144/sp483.6.

Searle, M.P., Waters, D.J., Parrish, R.R., Thow, A.V., Noble, S.R., Phillips, R.J., 2010. Anatomy, age and evolution of a collisional mountain belt: the Baltoro granite batholith and Karakoram Metamorphic Complex, Pakistani Karakoram. J. Geol. Soc. 167, 183–202. https://doi.org/10.1144/0016-76492009-043.Anatomy.

Shah, S.Z., Sayab, M., Aerden, D., Khan, M.A., 2011. Foliation intersection axes preserved in garnet porphyroblasts from the Swat area, NW Himalaya: a record of successive crustal shortening directions between the Indian plate and Kohistan-Ladakh Island Arc. Tectonophysics 509, 14–32.

Shah, S.Z., Sayab, M., Aerden, D., Iqbal, Q., 2012. Formation mechanism and tectonic significance of millipede microstructures in the NW Himalaya. J. Asian Earth Sci. 59, 3–13. https://doi.org/10.1016/j.jseaes.2012.05.001.

Skrzypek, E., Schulmann, K., Štípská, P., Chopin, F., Lehmann, J., Lexa, O., Haloda, J., 2011. Tectono-metamorphic history recorded in garnet porphyroblasts: Insights from thermodynamic modelling and electron backscatter diffraction analysis of inclusion trails. J. Metamorph. Geol. 29, 473–496. https://doi.org/10.1111/j.1525-1314.2010.00925.x.

St-Onge, M.R., Rayner, N., Palin, R.M., Searle, M.P., Waters, D.J., 2013. Integrated pressure-temperature-time constraints for the Tso Morari dome (Northwest India): Implications for the burial and exhumation path of UHP units in the western Himalaya. J. Metamorph. Geol. 31, 469–504. https://doi.org/10.1111/jmg.12030.

Suuronen, J.-P., Sayab, M., 2018. 3D nanopetrography and chemical imaging of datable zircons by synchrotron multimodal X-ray tomography. Sci. Rep. 8, 4747. https://doi.org/10.1038/s41598-018-22891-9.

Timms, N.E., 2003. Garnet porphyroblast timing and behaviour during fold evolution: Implications from a 3-D geometric analysis of a hand-sample scale fold in a schist. J. Metamorph. Geol. 21, 853–873. https://doi.org/10.1046/j.1525-1314.2003.00487.x.

Treloar, P.J., Palin, R.M., Searle, M.P., 2019. Towards resolving the metamorphic enigma of the Indian Plate in the NW Himalaya of Pakistan. Geol. Soc. Lond., Spec. Publ. 483, 255–279. https://doi.org/10.1144/sp483-2019-22.

Trouw, R.A.J., Tavares, F.M., Robyr, M., 2008. Rotated garnets: a mechanism to explain the high frequency of inclusion trail curvature angles around 90° and 180°. J. Struct. Geol. 30, 1024–1033. https://doi.org/10.1016/j.jsg.2008.04.011.

Whitney, D.L., Goergen, E.T., Ketcham, R.A., Kunze, K., 2008. Formation of garnet polycrystals during metamorphic crystallization. J. Metamorph. Geol. 26, 365–383. https://doi.org/10.1111/j.1525-1314.2008.00763.x.

Williams, M.L., Jercinovic, M.J., Hetherington, C.J., 2007. Microprobe monazite geochronology: understanding geologic processes by integrating composition and chronology. Annu. Rev. Earth Planet. Sci. 35, 137–175. https://doi.org/10.1146/annurev.earth.35.031306.140228.

Williams, P.F., Jiang, D., 1999. Rotating garnets. J. Metamorph. Geol. 17, 367–378. https://doi.org/10.1046/j.1525-1314.1999.00203.x.

Yeh, M.W., 2007. Deformation sequence of Baltimore gneiss domes, USA, assessed from porphyroblast Foliation Intersection Axes. J. Struct. Geol. 29, 881–897. https://doi.org/10.1016/j.jsg.2006.12.003.